Controlling encapsulation of charged molecules in vesicle-templated nanocontainers through electrostatic interactions with the bilayer scaffold

Mariya D. Kim, \* Sergey A. Dergunov, \*\* Eugene Pinkhassik\*\*

<sup>†</sup> Department of Chemistry, University of Connecticut, 55 North Eagleville Rd, Storrs, CT 06269-3060

Abstract: This work addresses the challenge of creating hollow nanocapsules with controlled amount of encapsulated molecules. Such nanocontainers or nanorattle-like structures represent an attractive platform for building functional devices, including nanoreactors and nanosensors. By taking advantage of electrostatic attraction between oppositely charged cargo molecules and the surface of templating bilayer of catanionic vesicles, formed by mixing single-tailed cationic and anionic surfactants, we were able to achieve substantial increase of the local concentration of molecules inside the vesicle-templated nanocapsules. Control of electrostatic interactions through changes in the formulation of catanionic vesicles or pH of the solution enabled fine-tuning of encapsulation efficiency in capturing ionic solutes. The ability to control the amount of entrapped molecules greatly expands the application of nanocontainers in the creation of functional nanodevices.

#### 1. INTRODUCTION

Hollow polymer nanocapsules with entrapped molecules are increasingly used in the construction of diverse functional nanodevices.<sup>1-14</sup> The ability to imprint uniform nanopores in the shells of vesicle-templated nanocapsules permitted tunable size- and charge-selective permeability, which translated into devices taking advantage of the ability to retain entrapped molecules while providing unhindered communication with the environment.<sup>4, 15-19</sup> For example, entrapment of homogeneous catalysts produced fast-acting and selective nanoreactors.<sup>1-2</sup> Encapsulation of indicator dyes has led to nanoprobes for sensing and imaging.<sup>3-4, 13, 18, 20</sup> Encapsulation offered further benefits, such as improved stability of photosensitive molecules and may lead to broader control of properties of entrapped molecules due to regulated microenvironment.<sup>4, 21-26</sup> In these applications, the underlying technology is based on nanocpntainers, or hybrid nanorattle-like structures, containing various molecules entrapped in the interior of a hollow nanocapsule with porous nanometer-thin shells.

Synthesis of these nanocontainers has immediate impact on the application of vesicle-templated nanocapsules. The entrapment of molecules into vesicle-templates nanocapsules is integrated into well-established procedures and the synthesis of nanocapsules.<sup>5, 17, 27-36</sup> In a typical synthetic approach, monomer-loaded vesicles are formed in the presence of target molecules in an aqueous solution followed by the polymerization of monomers and crosslinkers in the hydrophobic interior of the bilayer resulting in entrapment of molecules from the aqueous core of the vesicles (Figure 1).<sup>32</sup> The surfactant or lipid scaffold can be removed to yield hollow polymer nanocapsules with stable crosslinked shells. These nanometer-thin shells have intrinsic pores smaller than approx. 0.6 nm.<sup>33</sup> Larger pores can be imprinted in the shells by placing poreforming templates in the bilayer interior prior to the polymerization (Figure 1).<sup>1,15-17,19</sup> Molecules

that are located in the aqueous core of the vesicles remain entrapped in the nanocapsules if they are larger than the pores in the capsule shells.<sup>4, 15, 17-18, 33-34</sup> These vesicle-templated capsules showed remarkable stability, retaining entrapped molecules for five years without measurable leaching.<sup>13, 17</sup> Typically, the local concentration of the entrapped molecules inside the nanocapsules was identical to the concentration of the molecules in the aqueous stock solution used to prepare the vesicles for templating the nanocapsules.<sup>15</sup>

Controlling the encapsulation efficiency would be greatly beneficial for building nanocapsule-based devices. <sup>16-19</sup> The ability to alter local concentration compared with the stock solution will greatly expand the range of devices prepared by vesicle templating, e.g., previously reported nanoreactors and optical nanoprobes. Unfortunately, simply increasing the concentration of cargo molecules in the aqueous solution used for templating is not always feasible. For example, a common approach may include encapsulation of a water-soluble form of a catalyst or a ligand followed by solvent exchange for subsequent catalytic applications. We used this approach in the synthesis of nanoreactors. <sup>1-2</sup> Limited aqueous solubility of many organic molecules may impose limitations on the range of practical achievable concentrations of entrapped molecules. Also, for many molecules, increased concentration in water would interfere with the formation of a bilayer, thus jeopardizing the assembly of the nanocapsule shells.

This work aims at controlling the encapsulation of molecules through electrostatic interactions with the surfactant scaffold that is used for templating of nanocapsules. We hypothesized that attractive interactions between oppositely charged target molecules and ionic surfactants in the bilayer would increase the local concentration of target molecules inside the nanocapsules. This hypothesis is supported by previous studies reported by English et al. who showed that catanionic vesicles with a molar excess of the cationic surfactant (CTAT) efficiently

captured the anionic dye 5(6)-carboxyfluorescein (CF), cationic anti-cancer drug doxorubicin and retained it for very long periods of time.<sup>37</sup> To test this hypothesis, we selected six representative cationic and anionic molecules structures and sizes (Figure 1) and examined their encapsulation in nanocapsules template by catanionic vesicles. The catanionic vesicles are formed spontaneously by a combination of cationic and anionic surfactants.<sup>38-42</sup> In this study, we focus on vesicles formed by a cationic surfactant cetyltrimethylammonium tosylate (CTAT) and an anionic surfactant sodium dodecylbenzenesulfonate (SDBS).<sup>38-39</sup> Recently, we reported that SDBS/CTAT bilayers could be loaded with monomers during the vesicle formation stage (concurrent loading).<sup>32-33</sup> In the past, monomers were also placed into the bilayer by diffusion loading, where neat monomers were added to the aqueous dispersion of vesicles followed by an equilibration period, during which monomers diffused through water into the interior of a bilayer.<sup>28, 35-36, 43</sup> Polymerization of monomers can be conducted at physiological conditions using a peroxide initiator coupled with an activator co-dissolved in the bilayer,<sup>33</sup> or, alternatively, using UV irradiation.<sup>28, 34-35, 44</sup>

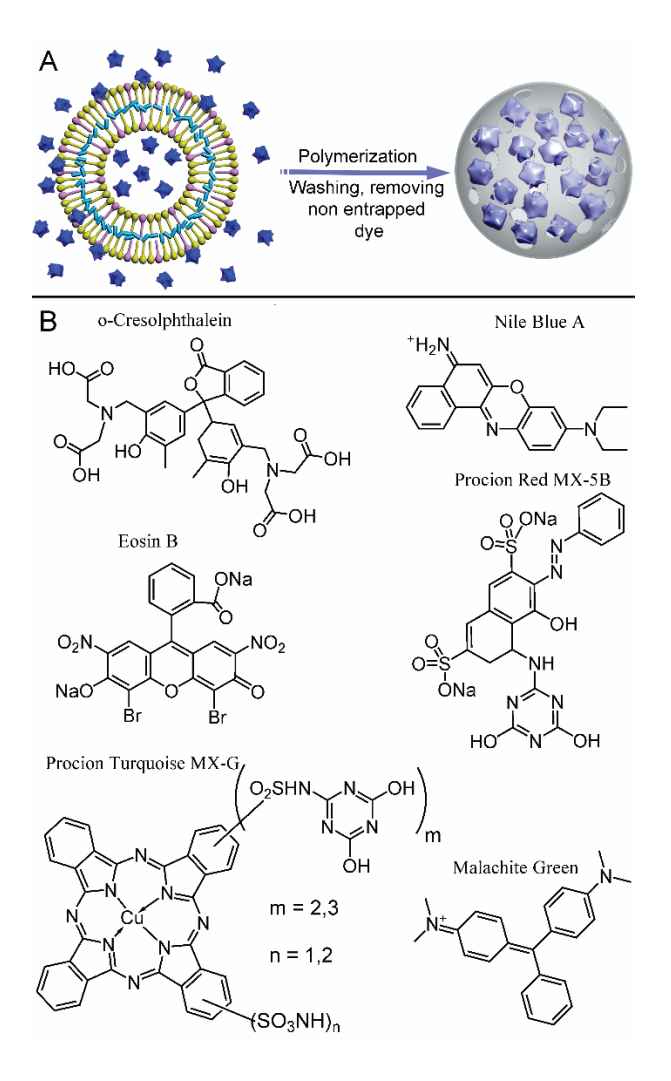


**Figure 1**. A) Schematic representation of vesicle-templated synthesis of nanocapsules: monomers and crosslinkers are loaded into the bilayers of spontaneously formed vesicles followed by the polymerization and removal of the vesicle scaffold and non-entrapped molecules. B) Structures of representative cationic and anionic molecules used for the investigation of entrapment efficiency regulated through electrostatic interactions.

# 2. EXPERIMENTAL SECTION

**Materials.** *Monomers:* butyl methacrylate (BMA), t-butyl methacrylate (t-BMA), ethylene glycol dimethacrylate (EGDMA) were received from Sigma-Aldrich. They were purified by

passing through aluminum oxide shortly before the synthesis. Sodium dodecylbenzenesulfonate (SDBS; an anionic surfactant), cetyltrimethylammonium p-toluenesulfonate (CTAT; a cationic surfactant), were used as received (Sigma-Aldrich). 2,2-dimethoxy-2-phenyl-acetophenone (DPA), purchased from Sigma-Aldrich, was used as photoinitiator. *Dyes:* Procion Turquoise MX-G (PT) (received from DyStar) and Procion Red MX 5B (PR) (received from Sigma-Aldrich) were deactivated in 0.1 wt% Na<sub>2</sub>CO<sub>3</sub> aqueous solution overnight at room temperature to substitute active chlorine atoms by hydroxyl groups<sup>45</sup>; o-Cresolphthalein (CPC), Nile blue A (NBA), Malachite Green, Eosin B (Sigma-Aldrich) used as received.

Concurrent loading of monomers into surfactant vesicles. To prepare stock solutions, SDBS (100 mg) and CTAT (100 mg) were mixed in separate vials with t-BMA (32 μL, 0.193 mmol), BMA (32 μL, 0.199 mmol), EGDMA (32 μL, 0.166 mmol) and initiator 2,2-dimethoxy-2-phenyl-acetophenone (3 mg, 0.01 mmol). Each mixture was hydrated in 10 mL of an aqueous solution of a dye. Each stock solution was incubated at 40 °C during 30 min, and vials were gently sonicated to break up chunks of aggregated surfactants and vortexed to homogenize solutions. Samples were prepared by mixing the stock solutions at proper volume ratios after brief vortexing. The solutions were not subjected to any further agitation and were extruded 5 times at 25 °C through a track-etched polyester Nucleopore membrane (Sterlytech) with 0.2 μm pore size using a Lipex stainless steel extruder (Northern Lipids).

**Synthesis of nanocapsules**. The sample obtained as described above was irradiated for 1.5 hours with UV light ( $\lambda$ =254 nm) in a photochemical reactor (10 lamps, 32W each; the distance between the lamps and the sample was 10 cm) using quartz tube with path length of light of approximately 3 mm. Following the polymerization, a solution of NaCl (0.02 mL of 3 N) in

methanol (10 mL) was added to the reaction mixture to precipitate the nanocapsules. The nanocapsules were separated from the reaction mixture and purified by repeated centrifugation and resuspension steps using first methanol (3 drops of 3M NaCl were added to aid precipitation), then water-methanol mixture, and finally pure water as washing solutions. Typically, after the first methanol/water wash, the supernatant became colorless. The lack of non-entrapped dyes on the supernatant was confirmed by UV-vis spectroscopy.

**Dynamic Light Scattering (DLS)**. Hydrodynamic diameter and polydispersity index (PDI) measurements were performed on a Malvern Nano-ZS Zetasizer (Malvern Instruments Ltd., Worcestershire, U.K.). The Helium-Neon laser, 4mW, operated at 633 nm, with the scatter angle fixed at 173°. The temperature was set at 25 °C. 80 μL samples were placed into disposable cuvettes without dilution (70 μL, 8.5 mm center height Brand UV-Cuvette micro). Each data point was an average of 10 scans. Data were processed using non-negative least squares (NNLS) analysis.

Electron microscopy images. To prepare the sample for SEM analysis (JEOL JSM-6335F, working voltage of 5 kV), a sample was placed on SEM pin stub specimen mount covered with double coated carbon conductive tabs and dried under vacuum. The studied samples were coated with a 7nm gold-palladium (60:40) layer using Polaron E5100 SEM Coating Unit. SEM were performed using the facilities in the UConn/FEI Center for Advanced Microscopy and Materials Analysis (CAMMA).

**Dye retention experiment.** A previously described colored size-probe retention assay was used to demonstrate successful formation of nanocapsules.<sup>15, 17, 19</sup> Molecules with different colors and sizes were encapsulated in surfactant vesicles, the polymerization was carried out, and

nanocapsules were separated from released size probes on a size-exclusion column and/or by precipitation of nanocapsules in methanol and purification by repeated centrifugation and resuspension steps using first methanol (3 drops of 3M NaCl were added to aid precipitation), then water-methanol mixture, and finally pure water as washing solutions. The precipitate was dried, and a portion of solid residue was weighted out (typically, 20-50±0.1 mg) and redispersed in a buffer to achieve a concentration of 0.125 wt.%. Buffers with different pH values were used for different dyes for consistency in measurements. The amount of retained dyes was measured by UV-vis spectroscopy as described below.

Optical spectroscopy. For the absorbance measurements of the dye-loaded nanocapsules an Olis SM 72 UV-vis spectrophotometer (Bogart, GA) was used in combination with an integrating cavity (Olis CLARiTY sample holder) used here to minimize the interference from light scattering in turbid samples. The CLARiTY accessory was equipped with 8 ml quartz cuvettes containing a "chimney" with an inner diameter of 10 mm. Samples were placed in custom-made quartz test tubes (QSI Quartz scientific inc.) with an outer diameter of 9.8 mm and volumes 2 mL that were inserted into the CLARiTY cuvettes. To ensure reproducibility in measurements, the same test tube was used for all measurements of a series of samples and the test tube was positioned the same way in the CLARiTY cuvette.

Steady-state fluorescence spectra were recorded on Cary Eclipse Fluorescence Spectrophotometer (Agilent). The photophysical data (steady-state absorption and fluorescence) of all free and encapsulated dyes were obtained in water and in buffer solutions at different pH values.

#### 3. RESULTS AND DISCUSSION

The underlying hypothesis of this study is that charged molecules would be preferentially entrapped in nanocapsules templated by vesicles containing an excess of surfactants of the opposite charge. Vesicles formed by catanionic surfactants require excess of one of the surfactants. As evident from previously published phase diagrams, such excess can vary from 20 to 80%, corresponding to the surfactant mixtures with molar ratios ranging from 60:40 to 90:10. Add as an overall positive or negative charge, we anticipate that charged molecules would be attracted to an oppositely charged bilayer, resulting in higher concentration of these molecules in the aqueous core of a vesicle compared with the bulk solution. Likewise, like-charged molecules would be repelled from the bilayer resulting in lower concentration than in the bulk solution. Once the vesicle is formed and formation of bilayer-templated shell is complete, the molecules in the aqueous core will remain entrapped in nanocapsules as long as they are larger than the pores in the shells. We have shown in our initial reports that once entrapped medium size molecules did not escape from the capsules for at least 5 years. As a containing an excess of surfactants of the surfactants require excess of surfactants of the surfactants require excess of surfactants of the opposite excess of one of the surfactants. As a containing an excess of surfactants of the opposite excess of one of the surfactants.

Choice of charged molecules for entrapment. To test the main idea of this work, we used six different cationic and anionic molecules shown on Figure 1. All of these molecules are dyes, a choice made to facilitate the measurements of the entrapped molecules. O-Cresolphthalein (CPC) is an anionic complexone indicator dye for calcium with an optimal performance at pH 10.<sup>51</sup> CPC is positively charged at low pH due to protonation of two amino groups, and negatively charged at higher pH (four carboxylic groups). Eosin B is a fluorescent compound that is neutral in strongly acidic conditions negatively charged at the pH above 4. Nile Blue A (NBA), a pH-sensitive indicator and a popular stain used in biology and histology, is positively charged in

neutral and acidic conditions. Malachite Green (MG) is a cationic dye. Nile Blue and Malachite Green are pH sensitive dyes, having cationic and neutral forms depending on pH. Procion Red (PR) and Procion Turquoise (PT) are anionic reactive molecules. These six molecules represent a broad spectrum of organic structures representative of molecular cargo that could be loaded into nanocapsules for making functional devices. The retention of dyes and encapsulation efficiency was determined for different pH and vesicles compositions using the procedure described in the Experimental Section. The concentration of dyes was in the range of 0.1-3 mM to avoid possible destabilization of vesicles at high dye concentrations.<sup>37,52-53</sup>

Synthesis of nanocapsules with entrapped cargo molecules. We conducted a series of experiments involving the synthesis of nanocapsules using different formulations of surfactants and dyes conducted at different pH values, followed by removal of non-entrapped dyes and measurement of dyes retained within the nanocapsules. In a typical synthesis, the monomers and crosslinkers were placed into the bilayer interior during self-assembly of vesicles (concurrent loading). After the spontaneous formation of monomer-loaded vesicles in the presence of charged dyes, solutions were extruded to narrow down the size distribution of vesicles. Monomers were polymerized using redox initiation at 40 °C. As shown previously, the polymerization was complete within two hours under these conditions.<sup>33</sup> Typical results are shown on Figure 2. The average sizes of colored nanocapsules isolated after the polymerization of monomers and measured by SEM (Figure 2B, average diameter from SEM data approx. 220±40 nm) matched the average sizes of vesicles with dyes observed by DLS (Figure 2A, average diameter from DLS data approx. 240±50 nm). In previous studies, we found that SEM served as a reliable method for confirming successful synthesis of spherical nanocapsules. Here we obtained SEM images for each sample as noted below to confirm the formation of nanocapsules at different formulations of surfactant scaffolds with different charged molecules and at different pH of the reaction mixture. SEM data showed that capsules preserved their spherical shape upon drying, similarly to hollow nanocapsules produced by using a UV-initiated polymerization and templated by liposomes<sup>15, 17, 19</sup> and surfactant vesicles.<sup>32, 34</sup> Typical correlogram obtained from the DLS measurements was close to a typical monomodal distribution (open circles in Figure 2A) suggesting that the predominant scattering occurred from vesicles. Typically, no evidence of large aggregates was found for acrylic monomers at used concentrations of dyes and surfactants.

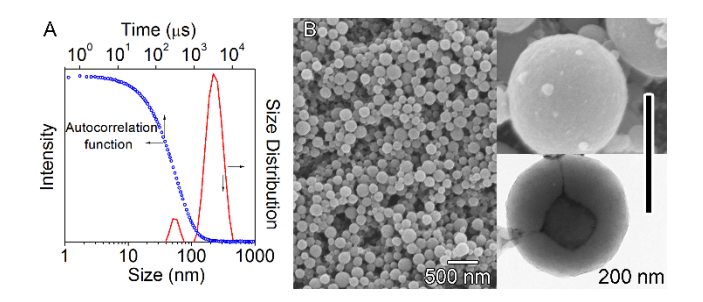


**Figure 2**. (A) Typical size distribution (solid lines) and autocorrelation function (open circles) of vesicles containing dye after polymerization determined by dynamic light scattering in aqueous solution; autocorrelation function indicates the correlation of scattering intensity at one time with itself at a different time, which is closely related to vesicles size. (B) Typical SEM image of nanocapsules after polymerization and template removal. Insets: SEM and TEM images of freestanding nanocapsules.

Effect of surfactant composition on the efficiency of entrapment. Following the general procedure outlined above, we conducted a series of experiments where yield and encapsulation ability of nanocapsules was measured as a function of the composition of vesicles. First, we

investigated the entrapment of NBA at a constant pH (5.8) and varying SDBS/CTAT ratio. At this slightly acidic pH, NBA is positively charged. We hypothesized that increasing amount of an anionic surfactant SDBS would lead to an increase of the amount of entrapped NBA due to attractive electrostatic interactions that would result in a greater local concentration of NBA inside the vesicles. The spectral data were normalized to the weight of the polymer material. Here and in the measurements shown on subsequent figures, we precipitated nanocapsules with methanol after the synthesis and washed the precipitate as described below. We then weighed out a certain amount of concentrated suspension of polymer material (to achieve the final concentration of nanocapsules of 0.125 wt. %) and redispersed it in a buffered aqueous solution for the absorbance measurements. The data shown on Figure 3A supported this hypothesis and revealed the general trend of increasing the amount of entrapped NBA with increased SDBS content. The data point corresponding to the 60/40 SDBS/CTAT mixture was an outlier. This composition is on the border between vesicles and two-phase region on the phase diagram and it is likely that monomer-loaded vesicles deteriorated during the synthesis, failing to produce a high yield of nanocapsules without pinhole defects.<sup>34</sup>

After the synthesis, nanocapsules were washed thoroughly with methanol and water to remove the surfactant scaffold, nonentrapped dyes, and buffer components. Washing steps were repeated multiple times until the supernatant showed no trace of non-entrapped dyes. Capsules with pinhole defects larger than the size probes would not be able to retain encapsulated molecules; therefore, the retention of the dyes is related to the yield of nanocapsules without pinhole defects. To account for possible variations in the overall yield of nanocapsules, we performed absorbance measurements on standard amounts of solid polymer material isolated from the synthesis as mentioned above.

The photographs (Figure 3B, C) show successive entrapment of dye in polymer nanocapsules produced from vesicles with varying SDBS/CTAT ratio. These data confirm that ionic dyes are efficiently captured in catanionic vesicles having an opposite net charge. However, vials 5-6 in the case of nanocapsules based on CTAT-rich vesicles have much lower dye content. Thus, the cationic NBA is efficiently incorporated into the nanocapsules based on SDBS-rich vesicles but not CTAT-rich vesicles. These data also showed that the total yield of colored nanocapsules was much higher for SDBS-rich vesicles. Similar results (highly efficient capture in nanocapsules based on SDBS-rich vesicles, and poor encapsulation in CTAT-rich vesicles) were obtained for MG, another cationic molecule (Figure S1).

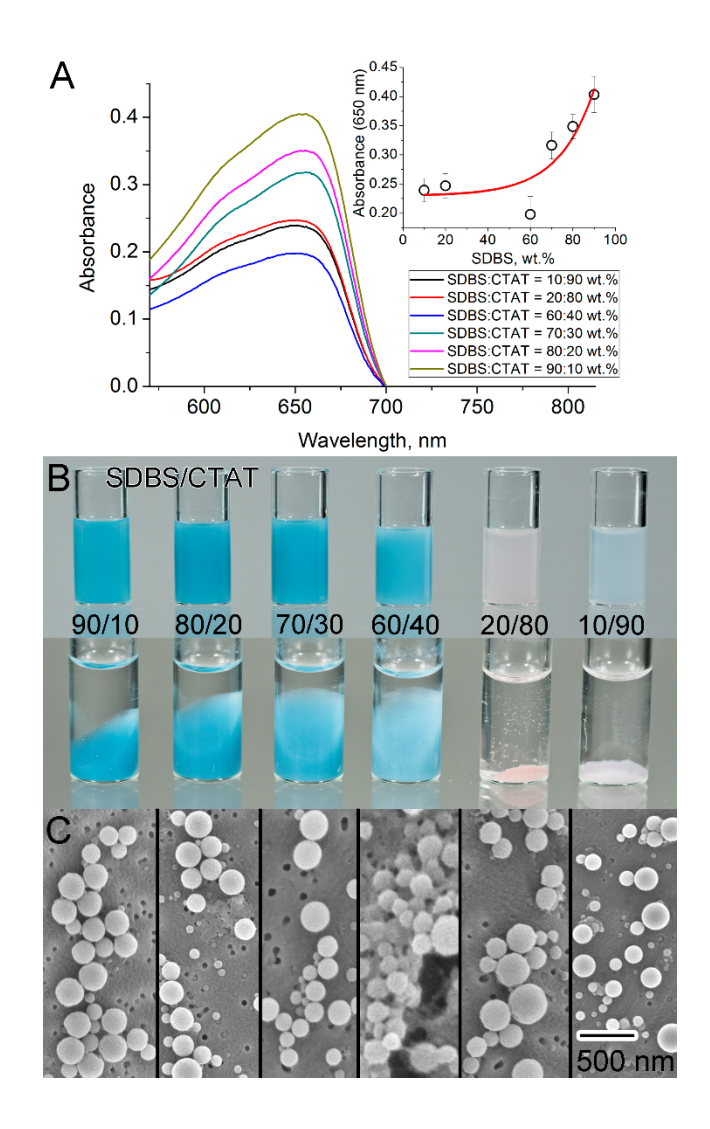


**Figure 3**. UV-Vis spectra (A), photograph of the aqueous suspensions (B, suspended (top) and precipitated (bottom) forms) and SEM images (C) of nanocapsules containing NBA synthesized at various ratios of SDBS:CTAT. Cm(NBA in reaction mixture) was 1.5x10<sup>-4</sup> M, pH of the reaction mixture was 5.8. Spectra were taken at pH 3.0 in sodium citrate buffer. Concentration of nanocapsules was 0.125 wt.% NC The inset shows the maximal absorbance at 650 nm versus various ratios of SDBS:CTAT. The line is a guide to the eye.

We obtained further confirmation of interactions between NBA and surfactant scaffold from fluorescence spectra of entrapped NBA. Figure 4 shows the emission spectra of encapsulated

NBA, taken from different compositions of surfactants, in acidic and basic environment. The emission spectra of NBA at both pH are also shown for comparison. Previously Douhal et al. showed that when NBA was excited at ~500 nm and two distinct fluorescence peaks were observed at ~590 and ~690 nm. 54 The former is attributed to the excited neutral form of NBA and the latter was assigned as fluorescence from excited cationic form of NBA, which is formed after an intermolecular proton transfer from the solvent. In our case, in basic conditions, we observed distinct dual fluorescence only for nanocapsules based on SDBS-rich vesicles. For nanocapsules based on CTAT-rich vesicles, we saw broad peak at ~600 nm with shoulder at ~670 nm. In acidic media, the emission peak for nanocapsules based on SDBS-rich vesicles was observed at 695 nm in good agreement with peak from free NBA, whereas for nanocapsules based on CTAT-rich vesicles the emission peak was blue shifted to 630 nm for composition 20:80 (SDBS:CTAT), and finally changed to two peaks at 621 and 667 nm when content of CTAT was at its highest value in the series of vesicles (10:90 SDBS:CTAT ratio). In addition, the emission intensity decreased slightly with increasing concentration of CTAT and then increased at the maximum CTAT content.

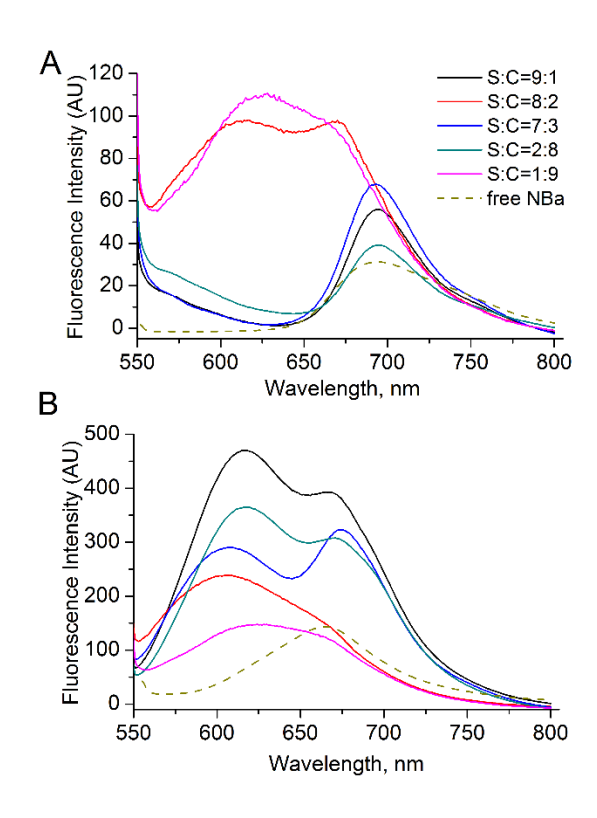


**Figure 4.** Steady-state fluorescence emission spectra of free and entrapped NBA. Ex.: 530 nm. Spectra were taken at pH 3.0 in sodium citrate buffer (A) and pH 10.0 in borate buffer (B). The concentration of nanocapsules was 0.125 wt.%.

Figure S2 depicts the pH-dependent emission spectra of entrapped NBA into nanocapsules obtained at different vesicles compositions measured at a fixed excitation wavelength of 530 nm. Entrapped NBA for all samples exhibits a positive pH dependence in the emission intensity with blue excitation, with more than a 5-fold increase between pH 3.5 and 12.5 for nanocapsules based on SDBS-rich vesicles, and 3-fold increase for nanocapsules based on CTAT-rich vesicles.

**Effect of pH on encapsulation efficiency**. Our reasoning was that pH would affect the interactions between the charged molecules and catanionic scaffold, translating into changes in the amounts of encapsulated molecules. This effect could be especially pronounced for pH-

sensitive molecules that change the charge upon protonation or deprotonation. We selected catanionic vesicles prepared from SDBS and CTAT at 80:20 weight ratio, which gave us higher yield of colored nanocapsules. Dynamic light-scattering (DLS) analysis revealed structures with an average diameter of 220±10 nm and a polydispersity index (PDI) of 0.2 – 0.4. For composition SDBS:CTAT = 80:20 wt.% (the middle of vesicles region for SDBS-rich vesicles)<sup>34</sup> the vesicle surface is predominantly negatively charged. We hypothesized that a cationic pH-sensitive molecule would exhibit higher encapsulation efficiency in its positively charged form in acidic solution compared with its neutral form in basic solution.

We used NBA, a cationic pH-sensitive dye, to test this idea. In water, when transitioning from basic to acidic media, NBA undergoes protonation at the primary and tertiary amino groups, changing from a neutral molecule to dicationic species. Using UV-vis spectroscopy, we measured the higher apparent pK<sub>a</sub> value of encapsulated NBA in water to be approx. 6.8. The discrepancy between the pK<sub>a</sub> values of free and encapsulated NBA was noted in our previous study<sup>4</sup> and will be discussed in detail separately. The lower pK<sub>a</sub> value for NBA was reported to be approx. 4. We chose four pH values for evaluating the effect of pH on encapsulation of NBA: 3.7, 4.9, 7.0, and 8.9. As noted previously, SDBS/CTAT vesicles are stable in the pH range that includes all selected values; therefore, we did not anticipate any negative effect of pH on the formation of nanocapsules. Our rationale for selecting specified pH values was that NBA was expected to be electroneutral at pH 8.9, a small fraction of NBA would bear a single positive charge at pH 7.0, nearly all molecules would possess a single positive charge at pH 4.9, and most of the molecules would exhibit a double positive charge at pH 3.7.

In these experiments, the stock solutions of NBA used to form vesicles were prepared at different pH values as indicated above. All other parameters, including the concentration of NBA and amounts of surfactants and monomers, were identical. After the synthesis of nanocapsules and removal of non-entrapped molecules, the pH of aqueous solutions was adjusted to a uniform value of 3 for all samples after the synthesis so as to compare the absorbance across all samples and correlate it with the amount of entrapped NBA. The photographs and absorption spectra of resulting suspensions of nanocapsules are shown on Figure 5, where pH values indicate the pH of the NBA stock solution used for the synthesis. Absorbance spectra (Figure 5A) show a large increase in absorbance with decreasing pH of solutions used in the synthesis of polymer nanocapsules. The correlation between the ionization state of NBA and absorbance data on Figure 5A suggests that the resulting concentration of NBA in nanocapsules is determined predominantly by the electrostatic interaction with the bilayer scaffold. At pH 8.9, NBA should be electroneutral, and no electrostatic attraction is expected between NBA and the predominantly negatively charged scaffold. At pH 7.0, a small fraction of NBA would have a positive charge, resulting in slight increase of attraction between NBA and the scaffold, which would translate into a slight increase of the amount of entrapped NBA. At pH 4.9, nearly all NBA molecules would possess a single positive charge, resulting in substantial increase in attraction between NBA and surfactant scaffold compared with neutral NBA. Further decrease of pH to 3.7 would render most of NBA molecules doubly charged due to protonation of both amino groups. This change translated in even stronger attraction between NBA and surfactant scaffold and higher amount of entrapped NBA. Figure 5b further illustrates increasing amount of entrapped dye corresponding to decreased pH values.

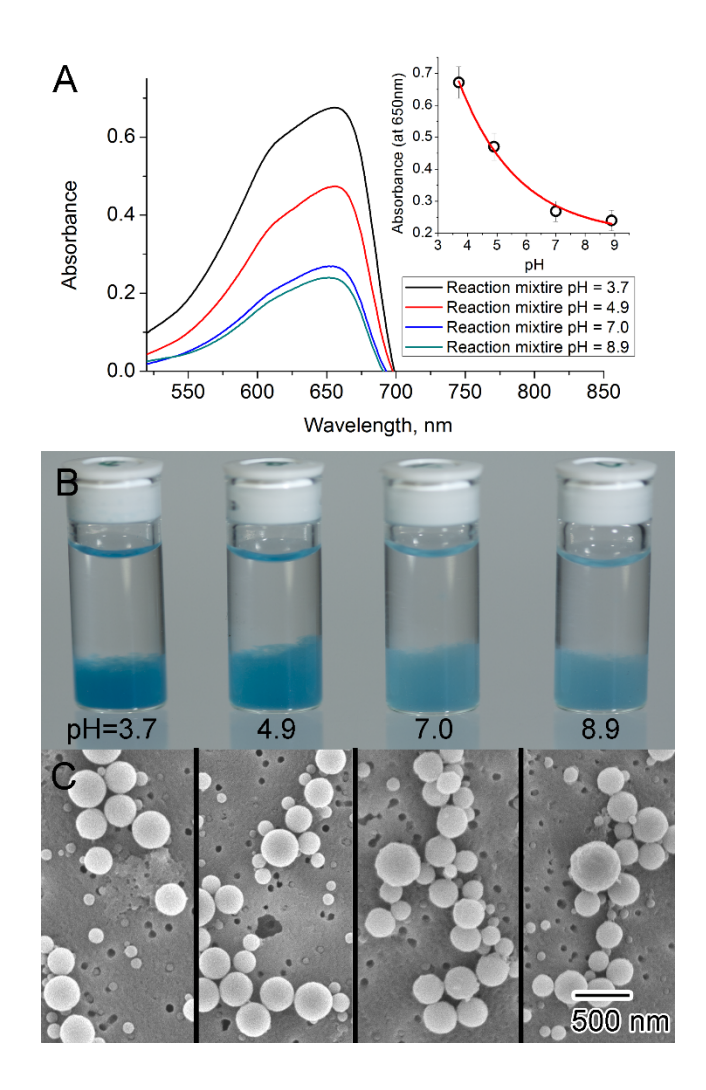


**Figure 5.** UV-Vis spectra (A), photograph (B) and SEM images (C) of nanocapsules containing NBA synthesized at various pH values. Concentration of nanocapsules was 0.125 wt.%, Spectra were taken at pH 3.0 in sodium citrate buffer. Nanocapsules were synthesized using 80:20 wt.% SDBS:CTAT vesicles. In all syntheses, the concentration of NBA in the reaction mixture was  $3x10^{-4}$  M. The inset shows the maximal absorbance at 650 nm versus pH during the synthesis.

For the anionic solutes (PR, PT, Eosin B, o-cresolephthalein), the results were reversed, and these dyes were efficiently captured in nanocapsules based on positively charged CTAT-rich vesicles and poorly captured in nanocapsules based on negatively charged SDBS-rich vesicles

(Figures 6 and 7). These data further confirm that ionic solutes are efficiently captured in nanocapsules based on catanionic vesicles having an opposite net charge of the bilayer. Nanocapsules with PT were synthesized at SDBS:CTAT=80:20 (Figure 6B), but in sample 2 the dye was added only to SDBS initial solution since PT was aggregated and precipitated in vesicles with high content on CTAT. Eosine B was encapsulated at two pH values, 3.3 and 4.4 (Figure S3). At higher pH, the synthesis of nanocapsules was not possible due to precipitation of the reaction mixture. Virtually no difference for encapsulation efficiency was found in this case, probably due to the same state of Eosin B at these pH values.

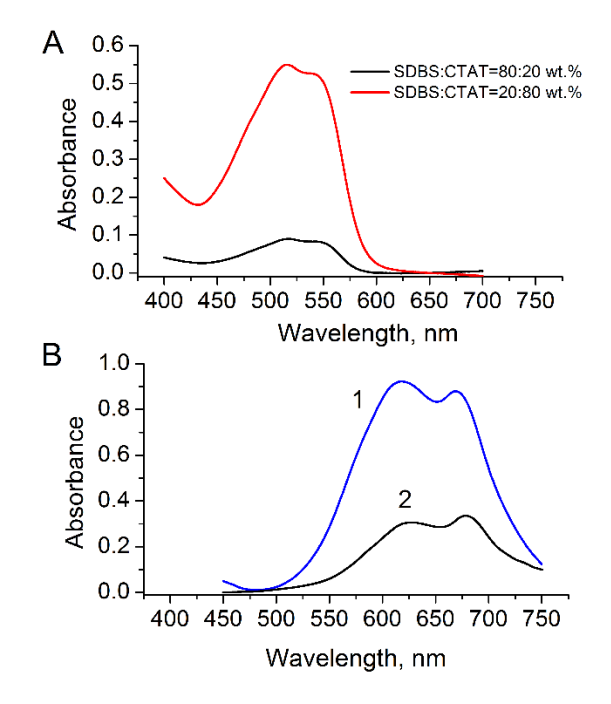


**Figure 6**. UV-Vis spectra of the suspensions of nanocapsules containing PR (A) and PT (B). Nanocapsules with PR were synthesized at various ratios of SDBS:CTAT. Nanocapsules with PT were synthesized at SDBS:CTAT=80:20, but in sample 2 dye was added only to SDBS initial solution. Cm(dyes in reaction mixture) was  $3x10^{-3}$  M, pH of the reaction mixture was 7.5. Spectra were taken at pH 7.5 in PBS. Concentration of nanocapsules was 0.125 wt.%.

CPC has four ionized carboxylic groups at pH values higher than its second pKa of 8.24. Synthesis of nanocapsules with CPC at pH 10.5 showed higher encapsulation efficiency for CTAT-rich compositions. We also evaluated encapsulation of CPC at different pH values for 20:80 wt % of SDBS:CTAT vesicles. In water, over the range of pH 8-12, CPC undergoes deprotonation at both phenol sites in addition to the carboxyl groups, changing it from a neutral molecule to multi-anionic species. It should be noted that CPC is not soluble in water at pH below 7. Figure 7 shows the photographs and absorption spectra of suspensions of nanocapsules with entrapped CPC (3 mM initial concentration of dye) in aqueous solutions at pH 12. In water at pH 12, deprotonation to form CPC leads to an increase in absorbance at  $\lambda$ >550 nm and appearance of purple-red color of dye. The photographs show successive encapsulation of dye in polymer nanocapsules obtained from CTAT-rich vesicles (Figure 7c). Thus, the anionic CPC is efficiently encapsulated into polymer nanocapsules based on CTAT-rich vesicles but not into the SDBS-rich ones.

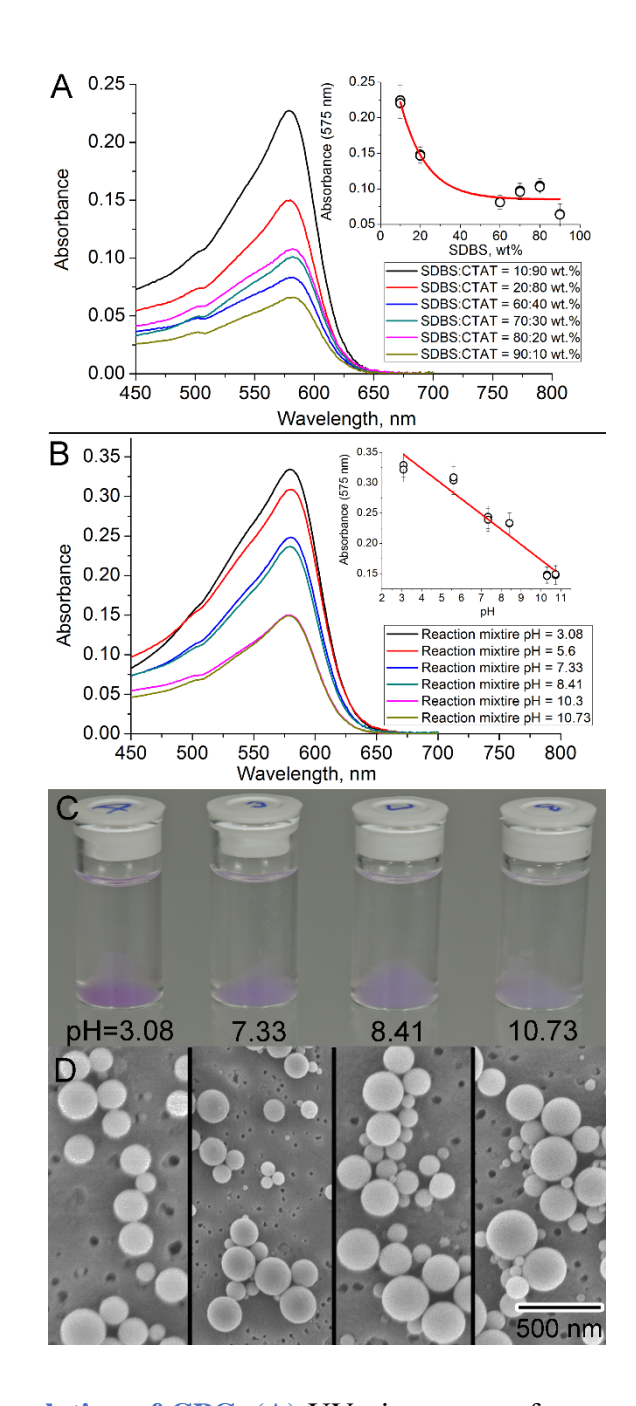


Figure 7. Data for encapsulation of CPC. (A) UV-vis spectra of nanocapsules prepared at pH 10.3 and varying composition of surfactant scaffold. Inset: maximum absorbance at 575 nm vs. SDBS content. (B) UV-vis spectra of nanocapsules prepared using 20:80 wt% of SDBS:CTAT vesicles at different pH values. Inset: maximum absorbance at 575 nm vs. pH, (C) Photographs and (D) SEM images of nanocapsules containing CPC synthesized at selected pH values using

20:80% SDBS:CTAT vesicles. Cm(CPC in reaction mixture) =  $3x10^{-4}$  M. Spectra were taken at pH 12 in Na<sub>2</sub>HPO<sub>4</sub> buffer. Concentration of nanocapsules was 0.125 wt. %.

Additional evidence for the electrostatic interactions between surfactant scaffold and entrapped cargo molecules dependent on pH and surfactant composition came from zeta potential measurements (Table S1). In these experiments, we observed the interactions between the bilayer and charged molecules located outside the vesicles. Blank vesicles showed expected values for zeta potential based on their composition, e.g., -108 mV for predominantly anionic 80:20 wt% SDBS:CTAT vesicles and +31 mV for predominantly cationic 20:80 wt% SDBS:CTAT vesicles. Upon addition of oppositely charged molecules, zeta potential values reduced dramatically, suggesting strong interactions between oppositely charged molecules and surfactants, e.g., +3 mV for 80:20 wt% SDBS:CTAT vesicles with NBA at neutral pH or -6 mV for 20:80 wt% SDBS:CTAT vesicles with CPC at pH 10. Varying the pH of solution of 20:80 wt% SDBS:CTAT vesicles with CPC suggested strong interactions between surfactants and CPC at basic pH as indicated above but not at acidic pH with zeta potential of +38 for 20:80 wt% SDBS:CTAT vesicles with CPC at pH 2.6, in line with expected attractions based on ionization of CPC at different pH values.

#### 4. CONCLUSIONS

In this study, we investigated the effect of electrostatic interactions between charged molecules and the bilayer of catanionic vesicles on the efficiency of entrapment of molecules in vesicle-templated nanocapsules. We tested the hypotheses that electrostatic attraction between

cargo molecules and the bilayer would translate in higher efficiency of encapsulation and that the encapsulation could be controlled by influencing the electrostatic attraction through the changes in the bilayer formulation or the pH of the solution. The experiments involved six representative charged dyes with different structures and catanionic vesicles formed with different amounts of CTAT and SDBS. Experimental evidence supported both hypotheses. Increasing electrostatic attraction due to change in pH or adjustment in formulation of surfactant scaffold did result in increased local concentration of encapsulated molecules compared with the stock solution. At the same time, electrostatic repulsion between cargo molecules and the bilayers has led to lower local concentration of encapsulated molecules. These findings demonstrate efficient control of encapsulation of cargo molecules inside nanocontainers based on hollow porous nanocapsules. A broad range of potential cargo molecules possesses a net charge, including most biomolecules, supporting the versatility of approach presented in this work. 55-56 The results of this work are likely to have an immediate impact on recently reported functional devices based on nanocapsules, including nanoreactors and optical nanoprobes, and enable or expand the range of other nanocapsule-based devices.

## **Corresponding Author**

\*Eugene Pinkhassik, eugene.pinkhassik@uconn.edu.

Sergey Dergunov, sergey.dergunov@uconn.edu

# **Author Contributions**

The manuscript was written through contributions of all authors. All authors have given approval to the final version of the manuscript.

## **ACKNOWLEDGEMENTS**

This work was supported by National Science Foundation (CHE-1709921, CHE-1522525). SEM studies were performed using the facilities in the UConn/FEI Center for Advanced Microscopy and Materials Analysis (CAMMA).

**Supporting Information**. This material is available free of charge via the Internet at http://pubs.acs.org

## **REFERENCES**

- 1. Dergunov, S. A.; Khabiyev, A. T.; Shmakov, S. N.; Kim, M. D.; Ehterami, N.; Weiss, M. C.; Birman, V. B.; Pinkhassik, E. Encapsulation of Homogeneous Catalysts in Porous Polymer Nanocapsules Produces Fast-Acting Selective Nanoreactors. *ACS Nano* **2016**, *10* (12), 11397-11406.
- 2. Ehterami, N.; Dergunov, S. A.; Ussipbekova, Y.; Birman, V. B.; Pinkhassik, E. Catalytic ship-in-a-bottle assembly within hollow porous nanocapusles. *New J. Chem.* **2014**, *38* (2), 481-485.
- 3. Zhegalova, N. G.; Dergunov, S. A.; Wang, S. T.; Pinkhassik, E.; Berezin, M. Y. Design of Fluorescent Nanocapsules as Ratiometric Nanothermometers. *Chemistry A European Journal* **2014**, *20* (33), 10292-10297.
- 4. Kim, M. D.; Dergunov, S. A.; Lindner, E.; Pinkhassik, E. Dye-Loaded Porous Nanocapsules Immobilized in a Permeable Polyvinyl Alcohol Matrix: A Versatile Optical Sensor Platform. *Anal. Chem.* **2012**, *84* (6), 2695-2701.
- 5. Ki, C. D.; Chang, J. Y. Preparation of a Molecularly Imprinted Polymeric Nanocapsule with Potential Use in Delivery Applications. *Macromolecules* **2006**, *39* (9), 3415-3419.
- 6. Kim, K. T.; Cornelissen, J. J. L. M.; Nolte, R. J. M.; van Hest, J. C. M. A Polymersome Nanoreactor with Controllable Permeability Induced by Stimuli-Responsive Block Copolymers. *Adv. Mater.* **2009**, *21* (27), 2787-2791.
- 7. Langowska, K.; Palivan, C. G.; Meier, W. Polymer nanoreactors shown to produce and release antibiotics locally. *Chem. Commun.* **2013**, *49* (2), 128-130.

- 8. Meeuwissen, S. A.; Rioz-Martinez, A.; de Gonzalo, G.; Fraaije, M. W.; Gotor, V.; van Hest, J. C. M. Cofactor regeneration in polymersome nanoreactors: enzymatically catalysed Baeyer-Villiger reactions. *J. Mater. Chem.* **2011**, *21* (47), 18923-18926.
- 9. Sauer, M.; Streich, D.; Meier, W. pH-Sensitive Nanocontainers. *Adv. Mater.* **2001,** *13* (21), 1649-1651.
- 10. Vriezema, D. M.; Comellas Aragonès, M.; Elemans, J. A. A. W.; Cornelissen, J. J. L. M.; Rowan, A. E.; Nolte, R. J. M. Self-Assembled Nanoreactors. *Chem. Rev.* **2005**, *105* (4), 1445-1490.
- 11. Vriezema, D. M.; Garcia, P. M. L.; Sancho Oltra, N.; Hatzakis, N. S.; Kuiper, S. M.; Nolte, R. J. M.; Rowan, A. E.; van Hest, J. C. M. Positional Assembly of Enzymes in Polymersome Nanoreactors for Cascade Reactions. *Angew. Chem. Int. Ed.* **2007**, *46* (39), 7378-7382.
- 12. Chen, Q.; Schönherr, H.; Vancso, G. J. Block-Copolymer Vesicles as Nanoreactors for Enzymatic Reactions. *Small* **2009**, *5* (12), 1436-1445.
- 13. Maclin, A. Q.; Kim, M. D.; Dergunov, S. A.; Pinkhassik, E.; Lindner, E. Small-Volume pH Sensing with a Capillary Optode Utilizing Dye-Loaded Porous Nanocapsules in a Hydrogel Matrix. *Electroanalysis* **2015**, *27* (3), 733-744.
- 14. Miksa, B. Recent progress in designing shell cross-linked polymer capsules for drug delivery. *RSC Advances* **2015**, *5* (107), 87781-87805.
- 15. Danila, D. C.; Banner, L. T.; Karimova, E. J.; Tsurkan, L.; Wang, X. Y.; Pinkhassik, E. Directed assembly of sub-nanometer thin organic materials with programmed-size nanopores. *Angew. Chem.Int. Edit.* **2008**, *47* (37), 7036-7039.
- 16. Dergunov, S. A.; Durbin, J.; Pattanaik, S.; Pinkhassik, E. pH-mediated catch and release of charged molecules with porous hollow nanocapsules. *J. Am. Chem. Soc.* **2014**, *136* (6), 2212-5.
- 17. Dergunov, S. A.; Kesterson, K.; Li, W.; Wang, Z.; Pinkhassik, E. Synthesis, Characterization, and Long-Term Stability of Hollow Polymer Nanocapsules with Nanometer-Thin Walls. *Macromolecules* **2010**, *43* (18), 7785-7792.
- 18. Dergunov, S. A.; Miksa, B.; Ganus, B.; Lindner, E.; Pinkhassik, E. Nanocapsules with "invisible" walls. *Chem. Commun.* **2010,** *46*, 1485-1487.

- 19. Dergunov, S. A.; Pinkhassik, E. Functionalization of Imprinted Nanopores in Nanometer-Thin Organic Materials. *Angew. Chem. Int. Ed.* **2008,** *47* (43), 8264-8267.
- 20. Dergunov, S. A.; Pinkhassik, E. Hollow Nanocapsules in Biomedical Imaging Applications. In *Nanotechnology for Biomedical Imaging and Diagnostics*; John Wiley & Sons, Inc, 2014, pp 83-109.
- 21. Isom, D. G.; Castaneda, C. A.; Cannon, B. R.; Garcia-Moreno, B. Large shifts in pKa values of lysine residues buried inside a protein. *Proceedings of the National Academy of Sciences of the United States of America* **2011**, *108* (13), 5260-5265.
- 22. Mehler, E. L.; Fuxreiter, M.; Simon, I.; Garcia-Moreno, E. B. The role of hydrophobic microenvironments in modulating pKa shifts in proteins. *Proteins* **2002**, *48* (2), 283-292.
- 23. Liu, N.; Higashi, K.; Kikuchi, J.; Ando, S.; Kameta, N.; Ding, W.; Masuda, M.; Shimizu, T.; Ueda, K.; Yamamoto, K.; Moribe, K. Molecular-Level Understanding of the Encapsulation and Dissolution of Poorly Water-Soluble Ibuprofen by Functionalized Organic Nanotubes Using Solid-State NMR Spectroscopy. *The Journal of Physical Chemistry B* **2016**, *120* (19), 4496-4507.
- 24. Pluth, M. D.; Fiedler, D.; Mugridge, J. S.; Bergman, R. G.; Raymond, K. N. Encapsulation and characterization of proton-bound amine homodimers in a water-soluble, self-assembled supramolecular host. *Proceedings of the National Academy of Sciences* **2009**, *106* (26), 10438-10443.
- 25. Brinker, U. H.; Mieusset, J.-L. *Molecular Encapsulation: Organic Reactions in Constrained Systems*. John Wiley & Sons, Hoboken, 2010; p 520.
- 26. Liu, J.; Qiao, S. Z.; Budi Hartono, S.; Lu, G. Q. Monodisperse Yolk–Shell Nanoparticles with a Hierarchical Porous Structure for Delivery Vehicles and Nanoreactors. *Angew. Chem. Int. Ed.* **2010**, *49* (29), 4981-4985.
- 27. Gomes, J. F. P. d. S.; Sonnen, A. F. P.; Kronenberger, A.; Fritz, J.; Coelho, M. Á. N.; Fournier, D.; Fournier-Nöel, C.; Mauzac, M.; Winterhalter, M. Stable Polymethacrylate Nanocapsules from Ultraviolet Light-Induced Template Radical Polymerization of Unilamellar Liposomes. *Langmuir* **2006**, *22* (18), 7755-7759.
- 28. Hotz, J.; Meier, W. Vesicle-Templated Polymer Hollow Spheres. *Langmuir* **1998**, *14* (5), 1031-1036.

- 29. Lai, W. C.; Tseng, S. C.; Tung, S. H.; Huang, Y. E.; Raghavan, S. R. Nanostructured polymers prepared using a self-assembled nanofibrillar scaffold as a reverse template. *J. Phys. Chem. B* **2009**, *113* (23), 8026-8030.
- 30. Ruysschaert, T.; Germain, M.; Gomes, J. F.; Fournier, D.; Sukhorukov, G. B.; Meier, W.; Winterhalter, M. Liposome-based nanocapsules. *IEEE Trans. Nanobiosci.* **2004**, *3* (1), 49-55.
- 31. Aguirre, G.; Ramos, J.; Heuts, J. P. A.; Forcada, J. Biocompatible and thermo-responsive nanocapsule synthesis through vesicle templating. *Polym. Chem.* **2014**, *5* (15), 4569-4579.
- 32. Dergunov, S. A.; Richter, A. G.; Kim, M. D.; Pingali, S. V.; Urban, V. S.; Pinkhassik, E. Synergistic self-assembly of scaffolds and building blocks for directed synthesis of organic nanomaterials. *Chem. Commun.* **2013**, *49* (94), 11026-11028.
- 33. Kim, M. D.; Dergunov, S. A.; Pinkhassik, E. Directed Assembly of Vesicle-Templated Polymer Nanocapsules under Near-Physiological Conditions. *Langmuir* **2015**, *31* (8), 2561-2568.
- 34. Kim, M. D.; Dergunov, S. A.; Richter, A. G.; Durbin, J.; Shmakov, S. N.; Jia, Y.; Kenbeilova, S.; Orazbekuly, Y.; Kengpeiil, A.; Lindner, E.; Pingali, S. V.; Urban, V. S.; Weigand, S.; Pinkhassik, E. Facile Directed Assembly of Hollow Polymer Nanocapsules within Spontaneously Formed Catanionic Surfactant Vesicles. *Langmuir* **2014**, *30* (24), 7061-7069.
- 35. McKelvey, C. A.; Kaler, E. W.; Zasadzinski, J. A.; Coldren, B.; Jung, H. T. Templating hollow polymeric spheres from catanionic equilibrium vesicles: synthesis and characterization. *Langmuir* **2000**, *16*, 8285 8290.
- 36. Morgan, J. D.; Johnson, C. A.; Kaler, E. W. Polymerization of Equilibrium Vesicles. *Langmuir* **1997**, *13* (24), 6447-6451.
- 37. Danoff, E. J.; Wang, X.; Tung, S.-H.; Sinkov, N. A.; Kemme, A. M.; Raghavan, S. R.; English, D. S. Surfactant Vesicles for High-Efficiency Capture and Separation of Charged Organic Solutes. *Langmuir* **2007**, *23* (17), 8965-8971.
- 38. Kaler, E. W.; Murthy, A. K.; Rodriguez, B. E.; Zasadzinski, J. A. Spontaneous vesicle formation in aqueous mixtures of single-tailed surfactants. *Science* **1989**, *245* (4924), 1371-1374.
- 39. Tondre, C.; Caillet, C. Properties of the amphiphilic films in mixed cationic/anionic vesicles: a comprehensive view from a literature analysis. *Adv. Colloid Interface Sci.* **2001,** *93* (1–3), 115-134.

- 40. Pucci, C.; Perez, L.; La Mesa, C.; Pons, R. Characterization and stability of catanionic vesicles formed by pseudo-tetraalkyl surfactant mixtures. *Soft Matter* **2014**, *10* (48), 9657-9667.
- 41. Silva, S. G.; Vale, M. L. C. d.; Marques, E. F. Size, Charge, and Stability of Fully Serine-Based Catanionic Vesicles: Towards Versatile Biocompatible Nanocarriers. *Chemistry A European Journal* **2015**, *21* (10), 4092-4101.
- 42. Kuo, A.-T.; Chang, C.-H. Recent Strategies in the Development of Catanionic Vesicles. *Journal of Oleo Science* **2016**, *65* (5), 377-384.
- 43. McKelvey, C. A.; Kaler, E. W. Characterization of nanostructured hollow polymer spheres with small-angle neutron scattering (SANS). *J. Colloid. Interf. Sci.* **2002**, *245*, 68-74.
- 44. Sierant, M.; Paluch, P.; Florczak, M.; Rozanski, A.; Miksa, B. Photosensitive nanocapsules for use in imaging from poly(styrene-co-divinylbenzene) cross-linked with coumarin derivatives. *Colloids and Surfaces B: Biointerfaces* **2013**, *111* (0), 571-578.
- 45. Dudman, W. F.; Bishop, C. T. Electrophoresis of dyed polysaccharides on cellulose acetate. *Can. J. Chem.* **1968**, *46* (19), 3079-3084.
- 46. Lee, C.-H.; Yang, Y.-M.; Leu, K.-L.; Lin, H.-Y.; Liang, C.-H.; Chang, C.-H. Exploring physical stability characteristics of positively charged catanionic vesicle/DNA complexes. *Colloid. Polym. Sci.* **2015**, *293* (8), 2239-2247.
- 47. Geng, S.; Wang, Y.; Wang, L.; Kouyama, T.; Gotoh, T.; Wada, S.; Wang, J.-Y. A Light-Responsive Self-Assembly Formed by a Cationic Azobenzene Derivative and SDS as a Drug Delivery System. *Scientific Reports* **2017**, *7*, 39202.
- 48. Jung, H. T.; Coldren, B.; Zasadzinski, J. A.; Iampietro, D. J.; Kaler, E. W. The origins of stability of spontaneous vesicles. *Proceedings of the National Academy of Sciences* **2001**, *98* (4), 1353-1357.
- 49. Brasher, L. L.; Kaler, E. W. A Small-Angle Neutron Scattering (SANS) Contrast Variation Investigation of Aggregate Composition in Catanionic Surfactant Mixtures. *Langmuir* **1996,** *12* (26), 6270-6276.
- 50. Wang, Z.; Leung, M. H. M.; Kee, T. W.; English, D. S. The Role of Charge in the Surfactant-Assisted Stabilization of the Natural Product Curcumin. *Langmuir* **2010**, *26* (8), 5520-5526.

- 51. Moorehead, W. R.; Biggs, H. G. 2-Amino-2-methyl-1-propanol as the Alkalizing Agent in an Improved Continuous-Flow Cresolphthalein Complexone Procedure for Calcium in Serum. *Clin. Chem.* **1974**, *20* (11), 1458-1460.
- 52. Caillet, C.; Hebrant, M.; Tondre, C. Sodium Octyl Sulfate/Cetyltrimethylammonium Bromide Catanionic Vesicles: Aggregate Composition and Probe Encapsulation. *Langmuir* **2000**, *16* (23), 9099-9102.
- 53. Marques, E. F.; Regev, O.; Khan, A.; Miguel, M. d. G.; Lindman, B. Interactions between Catanionic Vesicles and Oppositely Charged Polyelectrolytes Phase Behavior and Phase Structure. *Macromolecules* **1999**, *32* (20), 6626-6637.
- 54. Douhal, A. Photophysics of Nile Blue A in Proton-Accepting and Electron-Donating Solvents. *The Journal of Physical Chemistry* **1994,** *98* (50), 13131-13137.
- 55. Rosa, M.; Miguel, M. d. G.; Lindman, B. DNA encapsulation by biocompatible catanionic vesicles. *J. Colloid Interface Sci.* **2007**, *312* (1), 87-97.
- 56. Sciscione, F.; Pucci, C.; La Mesa, C. Binding of a Protein or a Small Polyelectrolyte onto Synthetic Vesicles. *Langmuir* **2014**, *30* (10), 2810-2819.

# TOC graphic

